DNA Origami Engineered Nanostructures: A Novel Method To Study Cell Signaling

Presented in fulfillment of the requirements for Undergraduate Research Distinction in Mechanical and Aerospace Engineering at The Ohio State University

Submitted by: Molly Mollica

2014

Faculty Advisor: Dr. Carlos Castro, Department of Mechanical and Aerospace Engineering

Co-advisor: Dr. Christopher Lucas, Post-Doctoral Researcher, Department of Mechanical and Aerospace Engineering

Thesis Committee: Dr. Carlos Castro & Dr. Robert Siston, Department of Mechanical and Aerospace Engineering

Abstract

The human body is composed of trillions of cells, which are the fundamental units of life. Understanding cell-cell communication is essential in developing effective therapies for a variety of diseases, including cancer. Current experimental approaches, such as ligands presented in solution, lack the ability to describe cell-cell communication because they do not accurately mimic ligand immobilization nor do they make it possible to examine the effects of ligand biophysical properties such as quantity or spatial arrangement. In order to better mimic ligand-receptor interactions during cell-cell communication, a novel nanotechnological device recently developed in the Nanoengineering Biodesign Laboratory. This device, called a Ligand Presentation Platform, is a DNA origami engineered structure that enables precise control over quantity and spatial arrangement of ligands presented to a cell surface. Precise structure folding and ligand attachment was confirmed using gel electrophoresis and transmission electron microscopy. Functional response was examined by adding nanostructures loaded with anti-CD40 antibody to B cells transfected with Cignal GFP-NF-κB reporter construct. A significant functional response up to 4-fold higher than relevant controls was observed via single cell epifluorescence. These results demonstrate that the Ligand Presentation Platform can induce a cellular functional response, making it possible to use the nanostructure to examine the influence of spatial arrangement and quantity to provide detailed mechanistic insight that can ultimately be utilized to design molecular therapeutics that target growth and survival signaling networks in cancer cells.

Acknowledgements

I would like to acknowledge and express my gratitude to my faculty advisor, Dr. Carlos Castro, and my post-doctoral researcher co-advisor, Dr. Christopher Lucas, for their assistance in the foundation of this project, its development, and all of the support and teaching that they performed to make the submission and defense of this thesis possible.

I would also like to thank my thesis committee faculty member, Dr. Robert Siston, for his willingness to be on my committee, his support of undergraduate research, and his assistance with my development in written and oral research presentation.

I would like to acknowledge and thank Team LPP: Randy Patton, Chris Lucas, and Emily Briggs for their assistance and persevering efforts on this project. Finally, I would like to thank all members of the Nanoengineering Biodesign Laboratory, past and present, for their support and research-loving attitudes.

Table of Contents

Table of Figures

Chapter 1: Introduction

1.1 Cancer and its Prevalence

The human body is composed of trillions of cells, which are the fundamental units of life. Under normal circumstances, healthy cells systematically grow, differentiate, replicate, and undergo apoptosis, or programmed cell death. This programmed death is a critical to maintain healthy populations of cells. Occasionally, cells mutate or become damaged and rather than undergoing apoptosis at an appropriate time, they become immortalized, begin to replicate uncontrollably, invade surrounding tissues, and ultimately interfere with normal organ system function, often leading to death. This disease phenotype is known as cancer.

Approximately 14 million people annually are diagnosed with cancer worldwide and approximately 8 million of these people will die of cancer[1]. In the US alone, a projected 1.6 million people will be diagnosed with cancer in 2014 and one in three diagnosed, or approximately 580 thousand Americans will die of this disease[2].

1.2 Cancer Therapies and Relevance of Ligand-Receptor Interactions

Major classes of cancer therapies include chemotherapy, radiotherapy, immunotherapy, and surgery. Ideally, these therapies would kill or remove cancer cells without harming healthy cells. However, since cancer cells are derived from healthy cells, differentiating between them is an intricate and difficult task.

Some therapies interfere with the function of a specific molecular target, such as a mutant kinase or extracellular protein, that exists on cancer cells at a higher rate than on

healthy cells. This target, usually a protein, is often critical in cell progression such that interfering with its function either halts cellular growth or destroys immortalized cells[3].

In order to develop the next generation of effective targeted therapies, molecular mechanisms that play a role in growth and survival must be well understood. Molecular mechanisms are often initiated by cell-to-cell contact in the form of a biochemical signal passed along by specific molecular interactions. A molecule, or ligand, on one cell engages a receptor on another cell. This molecular binding event initiates a chain of events that propagates a signal to ultimately execute a cellular response, such as growth or survival[4]. Understanding ligand-receptor interactions and the molecular mechanisms that these interactions govern allows for therapies to be developed to attack the growth and survival of cancer cells such that therapies that more effectively attack cancer can be developed.

1.3 Current Method to Studying Ligand-Receptor Interactions

The surface of cells possesses a variety of ligands and receptors that send and receive numerous signals. Due to the complexity of ligand-receptor interactions that coordinate communication, studying and understanding their mechanisms can be quite arduous. The current well-defined experimental approach to study these interactions includes presenting soluble ligands to cells and subsequently quantifying the functional cellular phenotypic and proximal molecular responses. However, physiologically, a cell is often presented ligands that are attached to a surface (e.g. cell membrane or tissue.) Therefore, soluble ligands often do not mimic a natural cell-cell interaction. While a ligand in solution can interact with cell surface receptors in a variety of conformations and orientations, a surface ligand, for example a cell

membrane, would engage a receptor in a more immobilized manner with physical support. The goal of this work is to test a more representative method of studying cell-signaling that includes the ability to properly immobilize the ligand and examine the influence of effects such as ligand spatial arrangement and ligand force or range of motion.

1.4 Introduction to DNA Origami

DNA (Deoxyribose nucleic acid) is composed of nitrogenous bases, five-carbon sugars, and phosphate groups. While DNA is well known for encoding biological information and forensic applications, intrinsic properties have allowed for the foundation of an entirely new field of bionanotechnology, structural DNA nanotechnology, where the assembly properties of DNA are exploited to construct objects with complex designed geometries.

The molecular structure of DNA, as shown below in Figure 1 and Figure 2, is a twisted ladder shape known as a double helix where the rungs of the ladder are formed by nucleotide bases, adenine (A), thymine (T), cytosine (C), and guanine (G), and the legs of the ladder are formed by the sugar-phosphate backbone. In addition, the assembly of the double helix is facilitated by hydrogen bonding in a manner such that the backbones of each strand run anti-parallel.

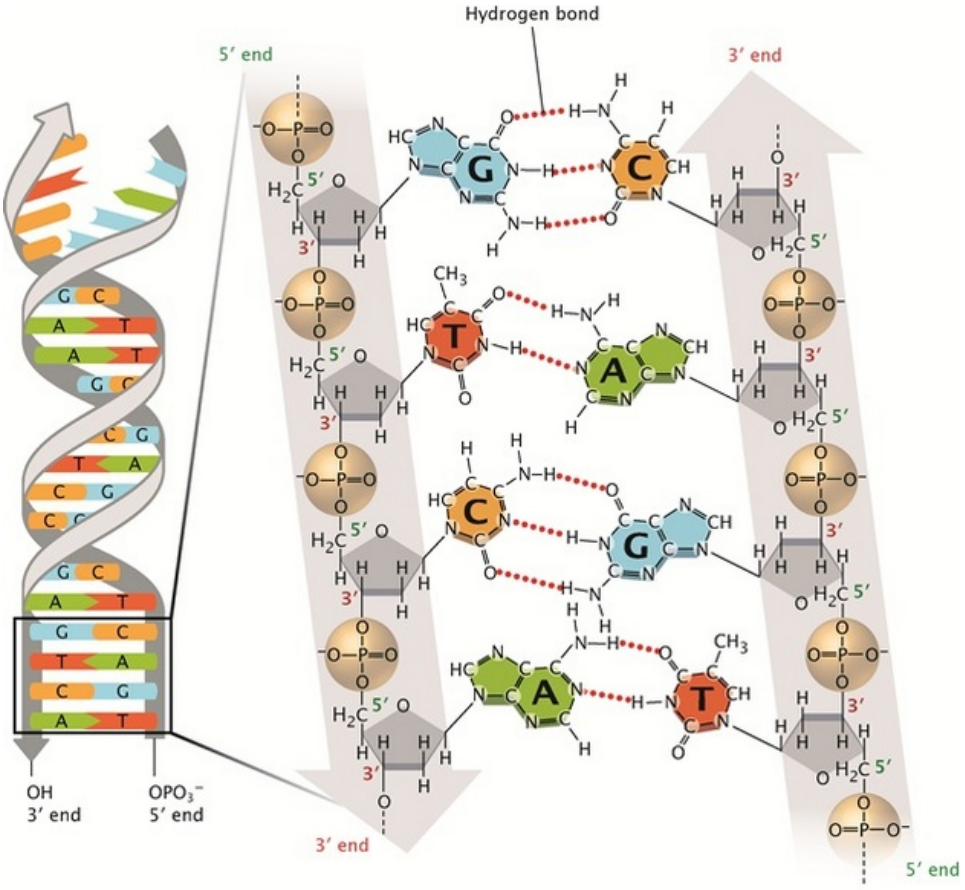

Figure 1: DNA Double Helix. DNA is a double helix, composed of antiparallel sugar-phosphate backbones joined by four nucleotides, depicted on the left. These nucleotides self-assemble such that A binds to T and C binds to G via hydrogen bonding. This self-assembly property is important in the foundation of DNA Origami.[5]

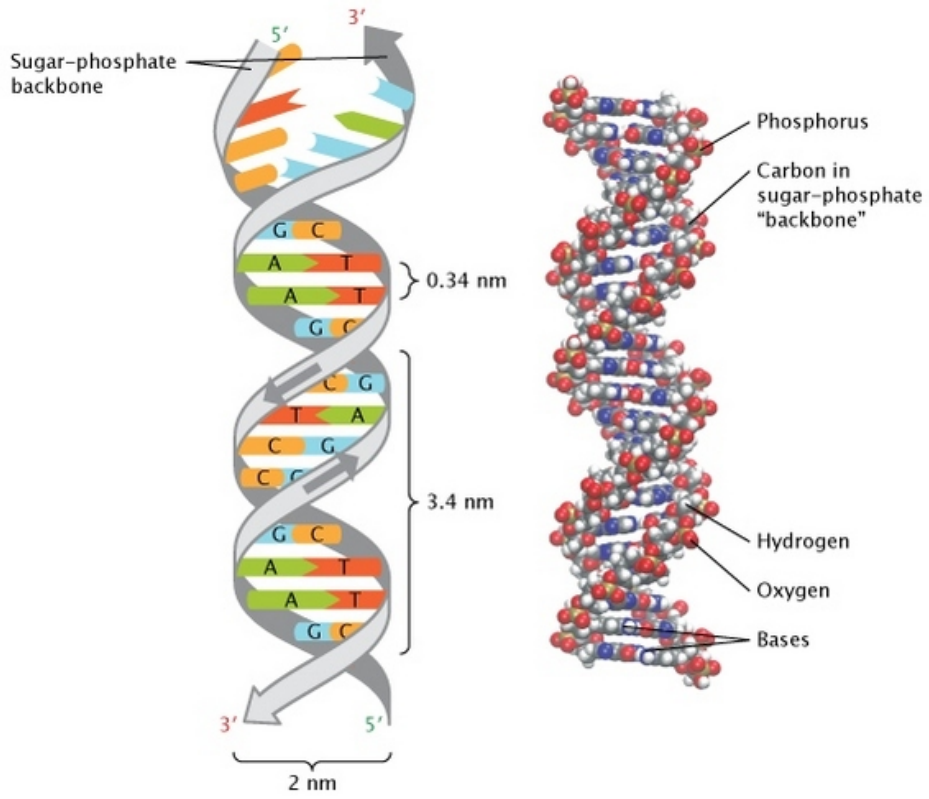

Figure 2: The structure of DNA's double helix is understood so precisely, that its dimensions are well-defined on the nanoscale. This structural property is important in the foundation of DNA Origami.[6]

The design and fabrication of DNA nanostructures exploits the well-understood assembly properties of nucleic acids to design two and three-dimensional nanoscale structures. The field of DNA nanotechnology was founded with Ned Seeman's work on nucleic acid junctions and lattices in the early 1980's[7] and his subsequent synthesis of a DNA molecule with cube connectivity in the early 1990's[8]. Since then, cumulative DNA nanotechnology related citations have been published at an exponential rate and a variety of shapes and functions have been proposed, as reviewed in "The enabled state of DNA nanotechnology."[9]

DNA origami is created by adding many 30-50 base single stranded DNA (ssDNA) oligomers to a long (~7000-8000 bases) circular ssDNA "scaffold" with a known sequence, such that the oligomers bind to the scaffold in a piece-wise manner to create a compact, high precision geometry as described in Figure 3. The scaffold is typically derived from the single-stranded genome of the M13MP18 bacteriophage. The sample is initially heated to melt all base-pairing interactions followed by slow cooling over several days to room temperature to facilitate annealing in a buffered solution with $MgCl_2$ to screen charge repulsions of the negatively charged backbone phosphate groups. The staples bind to the scaffold via complementary base pairing in a piece-wise manner to create a seemingly infinite number of possible 2D or 3D structures and a wide variety of functionalities that are commercial available. In this work, we will exploit the geometric precision of DNA origami as well as the ability to add chemical functionality in order to precisely control the number and spatial arrangement of ligands specific for cell surface receptors[10].

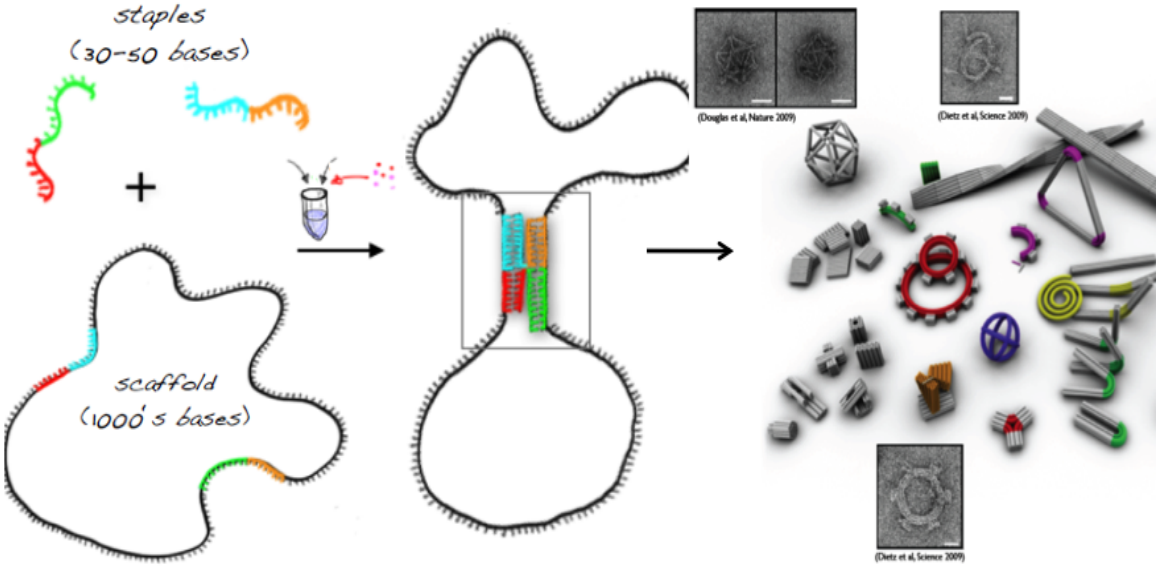

Figure 3: DNA Origami Functional Introduction. DNA origami is created by adding small strands of DNA (known as staples) to a single-stranded DNA molecule (known as scaffold.) Exploiting the complementary base pair connections, the staples will

attach to the scaffold, adjoining particular areas to create designed 2D or 3D structure. Images on right are courtesy of Hendrik Dietz, TUM.

1.5 Introduction to Ligand Presentation Platform

In order to better mimic a natural ligand-receptor interaction during a cell-cell interaction, it is possible to employ a novel nanotechnological device recently developed in Dr. Carlos Castro's laboratory in the Department Mechanical and Aerospace Engineering. This device is known as a Ligand Presentation Platform (LPP). An LPP is a 68 nm x 25 nm x 6 nm DNA origami structure[11,12] that is hypothesized to provide proper engagement configuration and physical support while introducing a ligand to cell surface receptors. This approach makes it possible to examine the influence biophysical properties of force[13], ligand quantity, and ligand spatial arrangements[14] because the 3 x 4 grid of potential ligand-binding biotinylated positions have a distinct DNA sequence, making it possible to attach any number of biotinylated ligands at any length from the platform. The biotinylated ligands can attach to the biotinylated nucleotide staple due to the addition of streptavidin and the high affinity of streptavidin for biotin. Streptavidin, which has four biotin binding sites, is used as a connector protein. As depicted in Figure 4, streptavidin attaches to the platform via a connection to the biotin staple and once streptavidin is attached to the platform, it still presents biotin binding sites to solution. This makes it possible to stably attach biotin-labeled ligands (biotinylated antibodies)[15] to the rigid DNA structure in any number and location.

With this design, as shown in Figure 5 and Figure 6, it is possible to properly immobilize ligand(s) and study the influence of the ligand quantity, spatial arrangement, and range of motion.

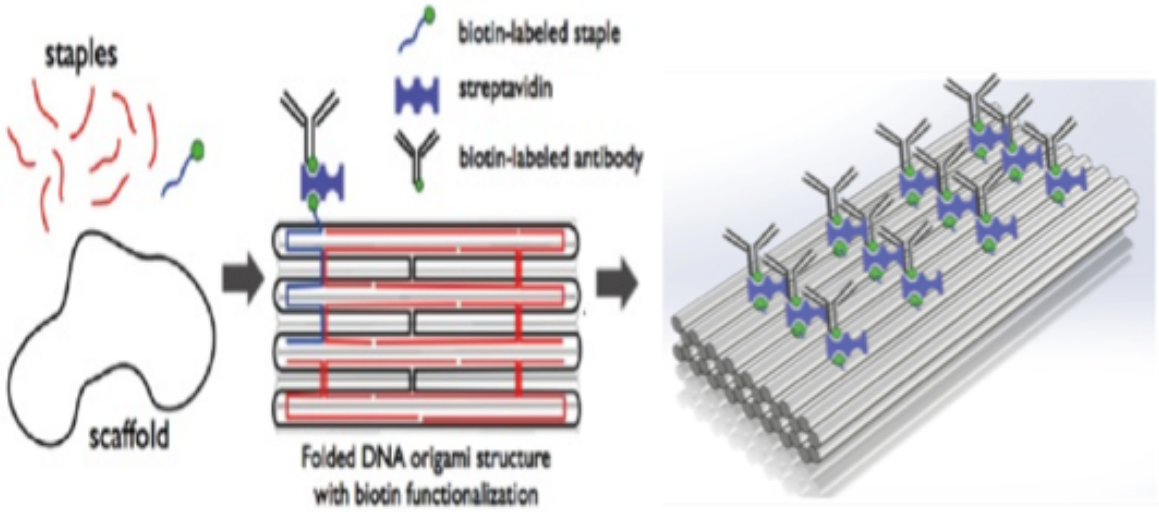

Figure 4: Ligand Presentation Platform functional introduction. A connector protein, streptavidin, is applied to attach a biotin-labeled staple to a biotin-labeled antibody. Twelve platform positions exist such that an antibody can be applied to any number and spatial configuration on the platform.

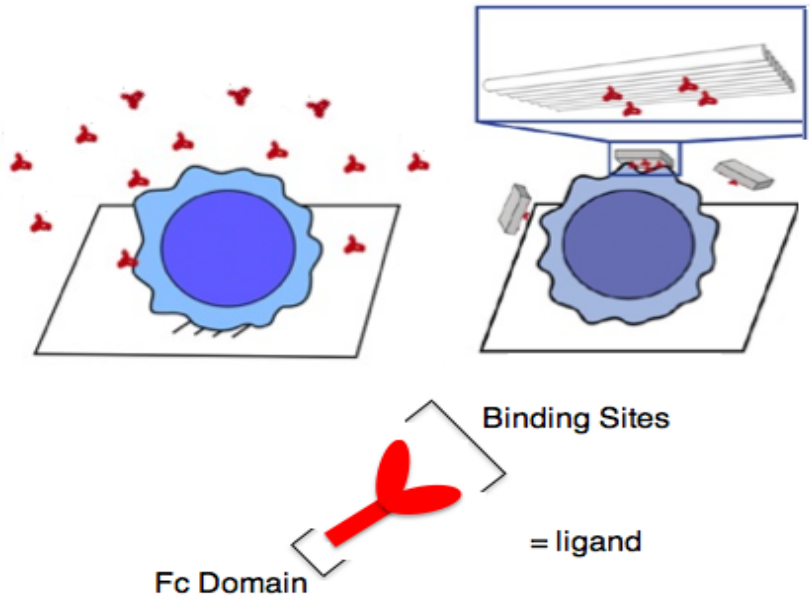

Figure 5: LPPs better mimic cell-cell interactions. An antibody "ligand" is often immobilized when engaging with a receptor. Current approaches (on left) often place ligands in solution and do not immobilize them. LPPs (on right) mimic a natural cell-cell reaction by immobilizing a ligand and allowing the ability to control ligand quantity and spatial arrangement.

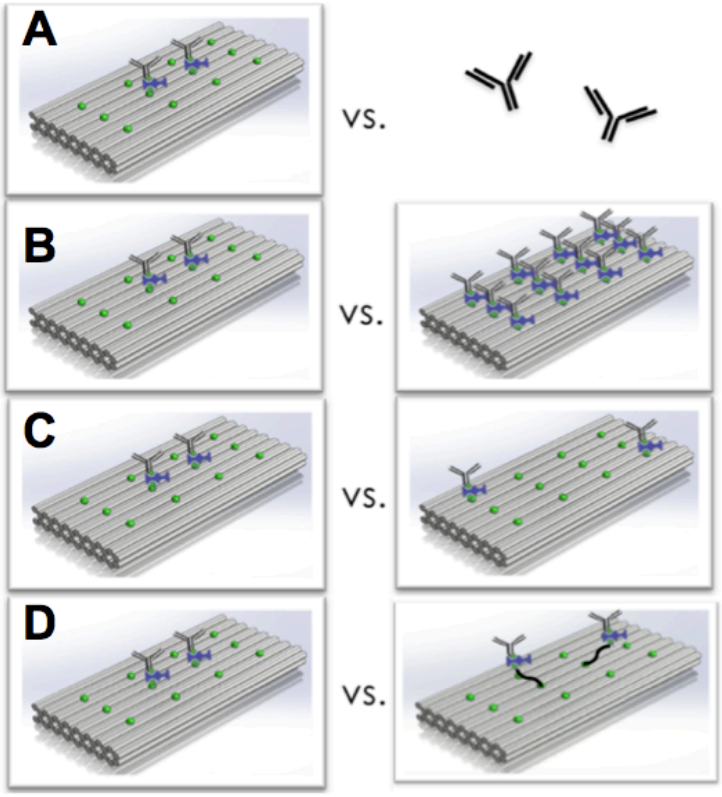

Figure 6: Using LPPs to study cell signaling. The Ligand Presentation Platform makes it possible to study the effect of the (A) Ligand Presentation Platform in comparison to the current experimental approach (ligands in solution), the effect of the (B) ligand number, the influence of the (C) spatial proximity of ligands, and (D) the effect of ligand support

1.6 Immune Cells: B Cells and T Cells

B and T lymphocytes are adaptive immune cells that work together to mount an immune response and protect the body from foreign pathogens. B cells are responsible for producing and secreting antibodies that specifically bind to a foreign antigen, halting the antigens ability to be harmful and flagging it for destruction. T cells fulfill multiple critical roles in an immune response. $CD4^+$ T helper cells identify antigenic peptide in association with major histocompatibility complex II (MHCII) on the surface of antigen-presenting cells and receive co-stimulatory signals to become fully active. Effector T helper cells help other immune cells such as B cells and macrophages function more effectively via secretion of specific soluble factors

known as cytokines. In addition, $CD8^+$ cytotoxic T cells recognize viral or tumor antigenic peptides in association with MHCI on the surface of virally infected cells or cancer cells and destroy the cells through perforin and granzyme B-mediated targeted lysis.[16] When B cells and T cells communicate via ligand-receptor interaction, a signal cascade occurs. That is, as shown in Figure 7, receptor engagement occurs and a system full of checks and balances is activated such that the engagement eventually leads to a cellular response.

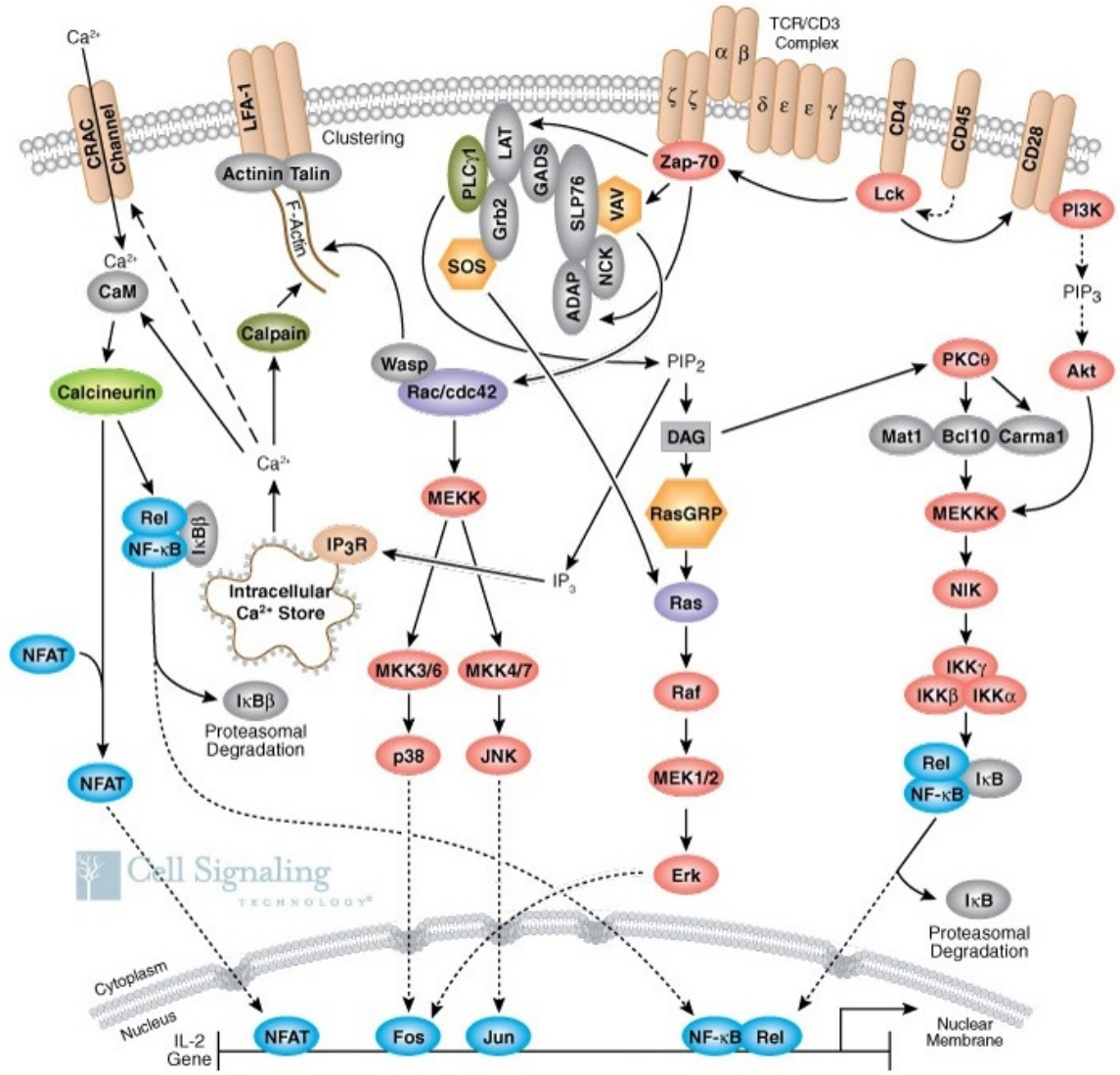

Figure 7: TCR/CD3 Signaling Cascade. This signaling cascade, activated by CD3 engagement of TCR, is an example of how ligation leads to a cascade of events that ultimately results in a cellular response.

Similar to the mechanism by which T cells become fully active, B cells must receive co-stimulatory signals from T cells to become high affinity antibody secreting plasma cells[17]. This is depicted in Figure 8. These co-stimulatory signals are mediated by receptors on the B cell surface, such as Cluster of Differentiation 40 (CD40.) CD40 is a well-studied stimulatory receptor on antigen presenting immune cells, including B cells[18,19]. CD40 signaling activates a wide variety of B cell functions including proliferation, survival signaling, cytokine and chemokine production, humoral immunity, antibody production, and a variety of other functions[20].

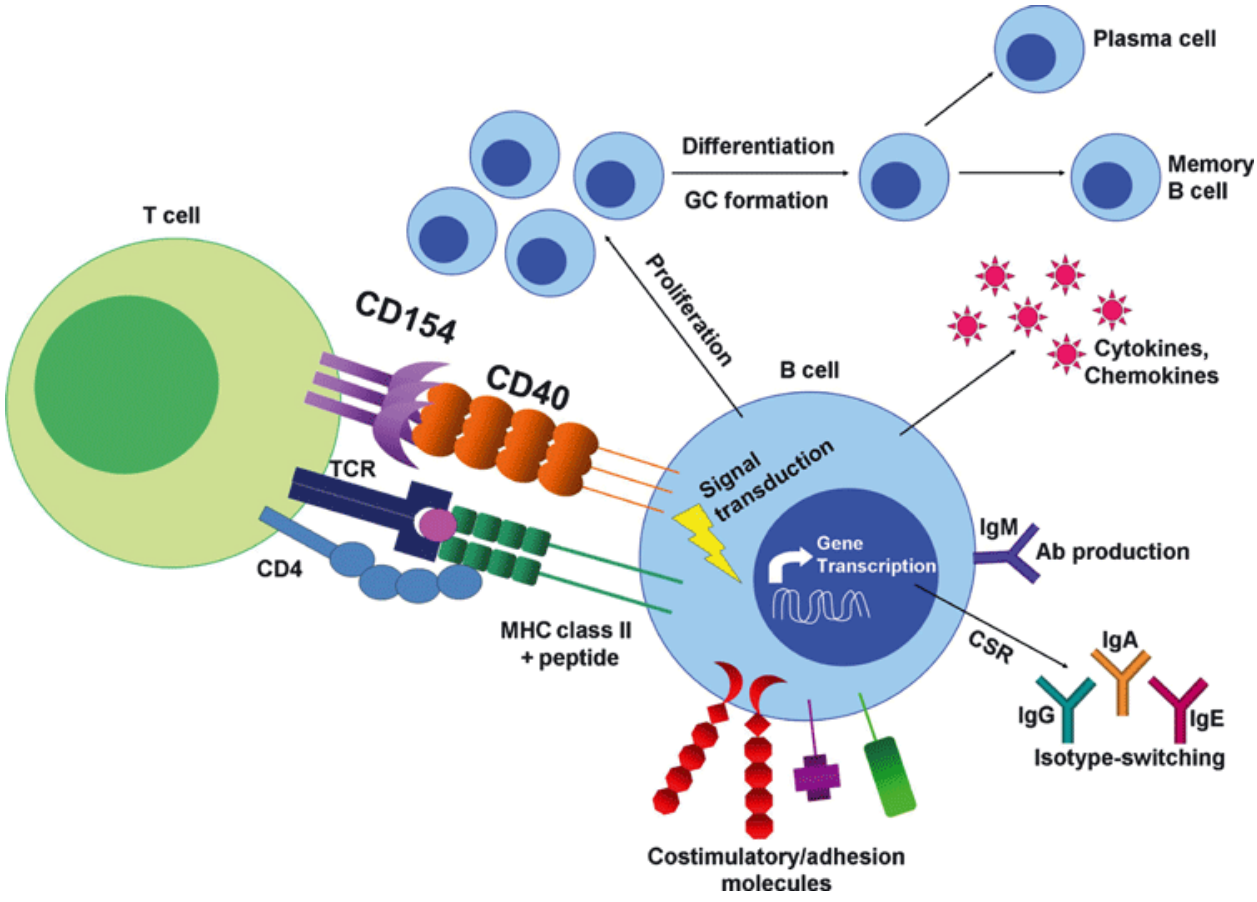

Figure 8: CD40 Engagement. B cell CD40 engagement by CD150 (CD40 Ligand) induces a variety of relevant signaling functions including proliferation, cytokine and chemokine production, antibody production, and isotype switching. The proliferation and pro-survival signals are especially relevant in cancer biology.[21]

These cellular responses are governed through major changes in gene expression controlled by the activation of molecules known as transcription factors. Nuclear Factor Kappa B (NF-κB) is one transcription factor that is activated via CD40 signaling. This transcription factor plays several roles in the immune system, including expression of growth factors, cytokines, and apoptosis inhibitors.[22] Whether referring to the classical or nonclassical pathway (as describe in Figure 9), dysfunction of this activation is thought to play a critical role in proliferation, migration, and apoptosis resistance in cancer.[23]

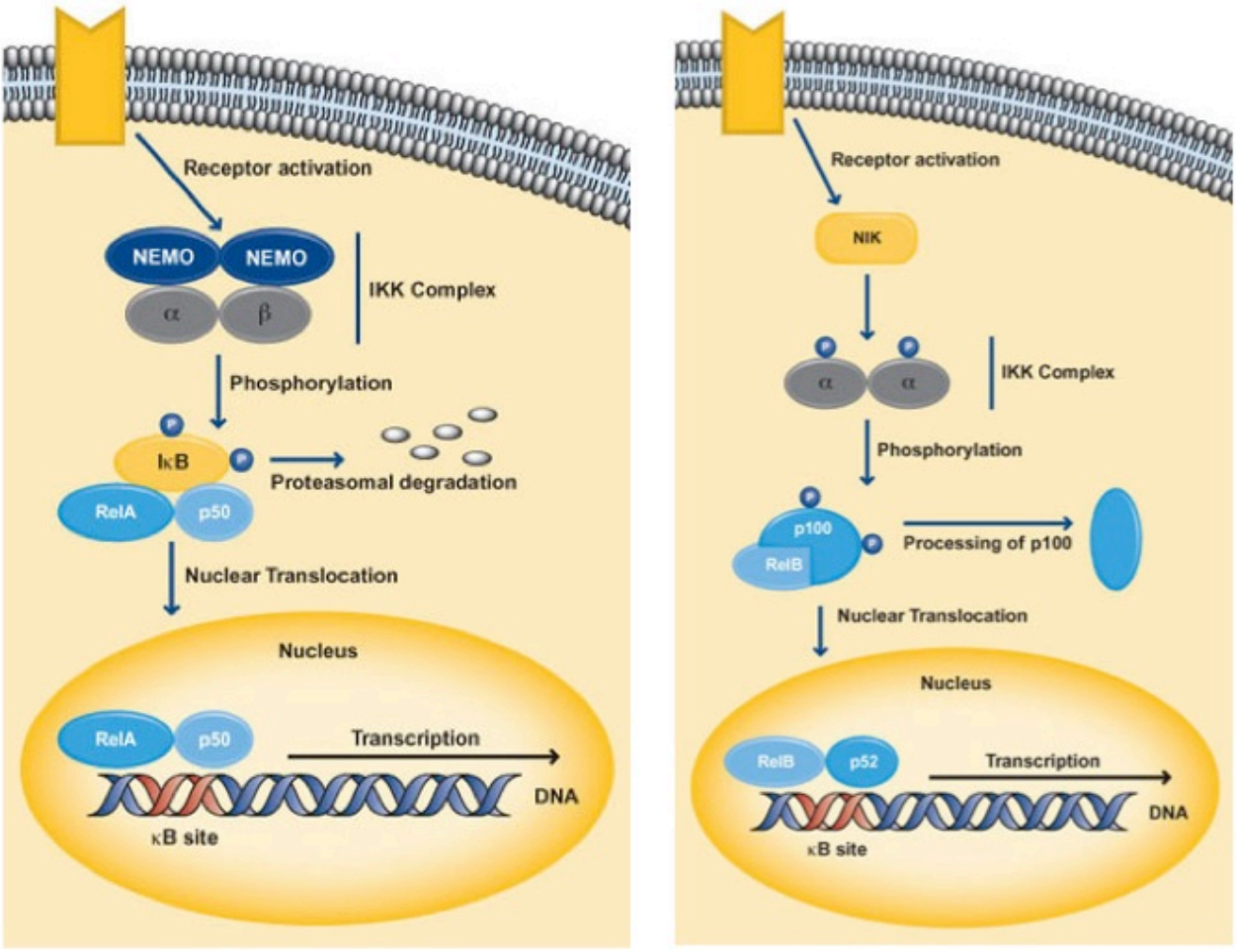

Figure 9: The classical pathway (left) employs the activation of IkB kinase (IKK) complex and NF-kB essential modulator (NEMO.) IKK phosphorylates IkB, causing proteasomal degradation. This then undergoes nuclear translocation and activates target genes. The nonclassical pathway (right) employs the activation of NF-kB inducing kinase (NIK.) NIK phosphorylates IKK alpha that phosphorylates IkB. This then undergoes nuclear translocation to and activates target genes.[24]

Similarly to CD40 on B cells, the T cell antigen receptor complex (TCR), expressed on T cells, has been extensively studied and its activation and signaling is relatively well understood[25], making it a good model system in instituting a novel method to better understand ligand-receptor signaling in cell types relevant to cancer and other signaling-related disease phenotypes. Particularly relevant to this work, the importance of biophysical characteristics of density and force on TCR activation have been recognized. The TCR is a

mechanoreceptor activated by the costimulation of CD3 and CD28. In addition to activation via stimulation of CD3 or costimulation of CD3 and CD28, clustering of TCRs upon engagement is a well-known phenomenon that is believed to enhance signaling[26]. Finally, it has been established that TCR is a mechanoreceptor that requires a ligand to provide mechanical force for engagement[27,28].

Upon T cell engagement, a signaling cascade occurs that includes an intracellular calcium flux (see Figure 9.) Calcium is a secondary messenger molecule stored in the sarcoplasmic reticulum. Due to recruitment of calcium after the hydrolysis of phosphatidylinositol 4,5-bisphosphate to inositol 3,4,5-triphosphate (IP_3), intracellular calcium flux occurs upon T cell activation and measuring this flux can be used as an indicator of receptor activation[29,30,31]. In addition, relevant to mounting an effective immune response, activation leads to Interleukin 2 (IL-2) production and T cell proliferation and differentiation[32,33,34]. Together, with their relevance to cancer signaling[35,36], these well-defined signaling networks provide excellent models to test and develop a novel tool to study cancer-relevant cell signaling.

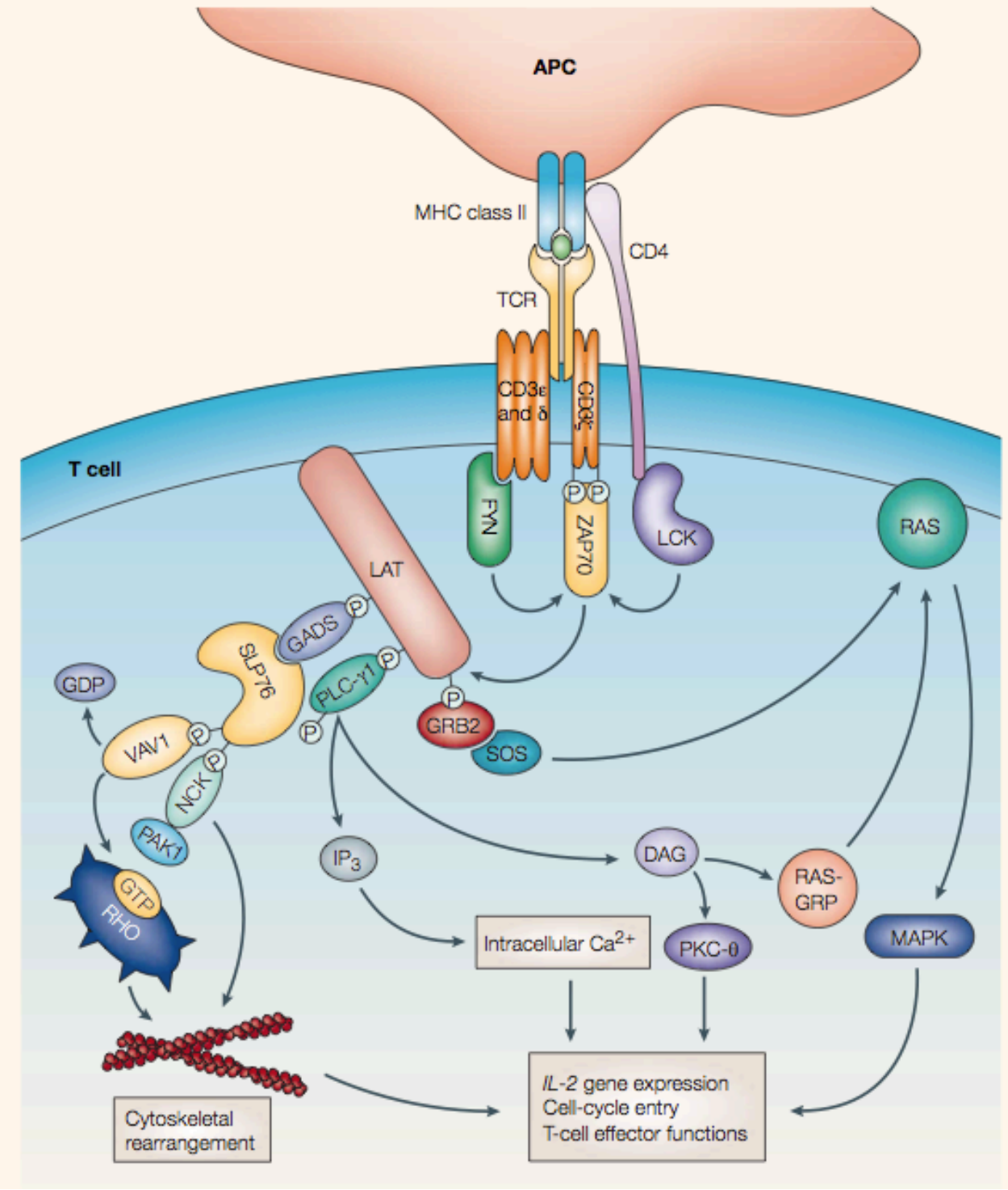

Figure 10: TCR Activation is a well-defined signaling pathway that includes phosphorylation of CD3 molecules, activation of protein tyrosine kinases, phospholipase C-γ1 (PLC-γ1), hydrolysis of phosphatidylinositol 4,5-bisphosphate to inositol 3,4,5-triphosphate (IP_3.) This increases intracellular calcium and IL2 gene expression. Image courtesy of Abraham and Weiss.

1.7 Significance

Reduction in cancer death rates in the last two decades has lead to over 1 million projected lives saved. Over the last five years with available data, cancer death rates in women have decreased by 1.6% per year while cancer death rates in men have decreased 1.8% per year. These decreases in death rate and these projected saved lives are largely due to more effective diagnostics and treatments. However, in the United States alone, 1.6 million new cancer diagnoses and over 580 thousand cancer deaths occur per year. Tragically, almost one in two men one in three women are diagnosed with cancer and one in four Americans die from cancer[37].

The establishment of a more representative procedure to study pro-growth and survival cell signaling which may also be applied to death receptor signaling will allow cellular communication to be examined on an individual cellular and molecular basis, providing mechanistic information and a more thorough understanding of activation and signaling pathways. Broadened understanding of these signaling cascades and detailed mechanistic information can ultimately be utilized to design molecular therapeutics that target growth and survival signaling networks in cancer cells, increasing therapeutic potential.

1.8 Thesis Objective and Hypothesis

The objective of this thesis is to better understand cell-cell communication that facilitates growth and survival by examining the effects of ligand immobilization, spatial arrangement, and biophysical characteristics. This is because better understanding of growth

and survival signaling will lead to the development of effective targeted therapies to treat cancer.

To do this, it is hypothesized that ligand spatial arrangement, linker length, and quantity can be controlled on a DNA origami engineered nanostructure. Ultimately, a method to study ligand-receptor interactions that includes all of these factors will lead to increased understanding of cell communication, thereby increasing therapeutic potential in cancer and other diseases.

1.9 Thesis Overview

This thesis includes four chapters: chapter 1 is the introduction and relevant background, chapter 2 includes methodology, chapter 3 details results, and chapter 4 discusses conclusions and future work. Each chapter is separated into subchapters marked by the chapter number, a period, and the subchapter. If this is being accessed digitally, a click-able table of contents exists at the beginning of the document, on page iv. A table of figures exists on page v. References are included on the final pages of the document.

Chapter 2: Ligand Presentation Platform Methodology

2.1 Design

The rigid platform basis for the LPP was designed using caDNAno[38] such that twelve binding sites exist in a 3 x 4 grid. Each binding site is composed of a biotinylated staple with a specific and distinct DNA sequence, which determines its location within the structure. This site specificity allows for inclusion or exclusion of ligand attachment sites at any of the twelve locations. Furthermore, the length of the overhang on the biotinylated staples can be individually controlled. Figure 11 shows the design of the structure. The scaffold is shown in blue and the twelve binding sites are depicted in green.

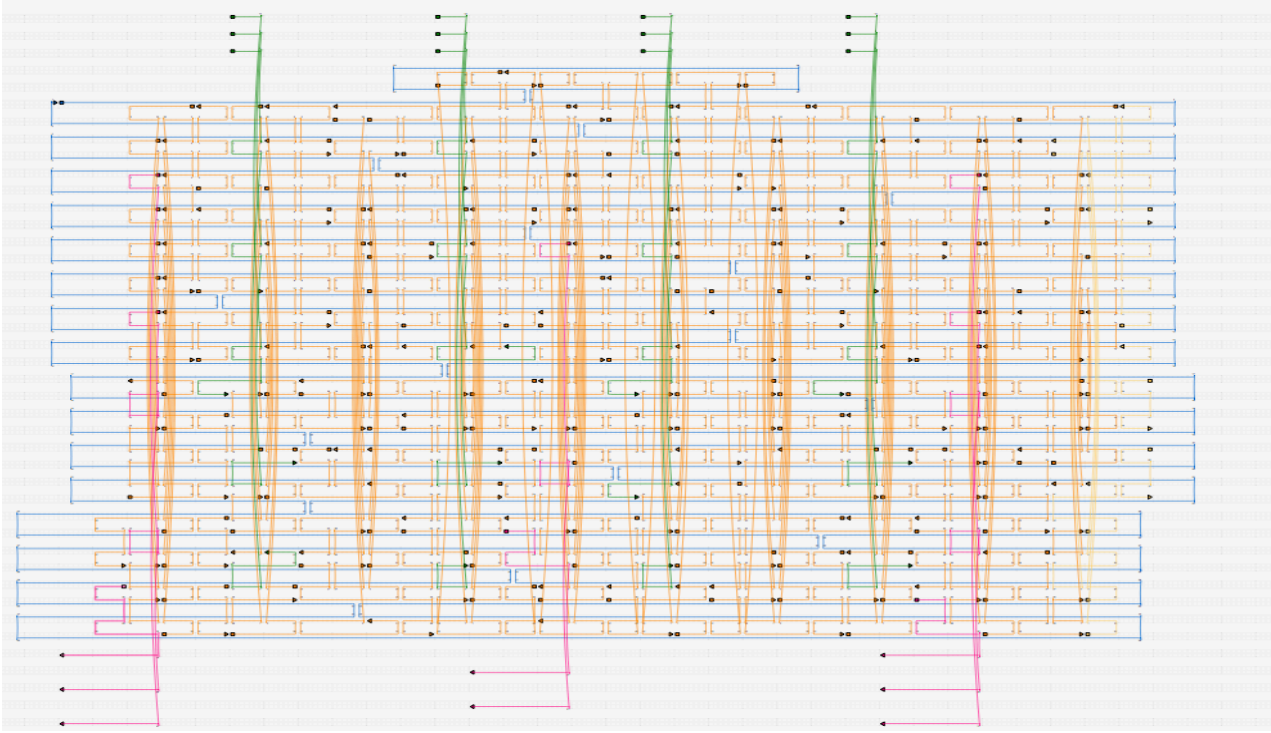

Figure 11: caDNAno 2 Design. The Ligand Presentation Platform was designed using caDNAno. Its twelve binding sites are depicted in green. This structure was originally designed by Emily Brigs, M.S. in the Nanoengineering Biodesign Lab.

2.2 Folding Reaction and Purification

The platform was folded using DNA origami methods previous defined in "A primer to scaffolded DNA Origami[39]." Specifically, a 7560 base scaffold derived from the M13mp18 ssDNA genome was placed in solution at 30 nM with 1X Folding Buffer, 20mM $MgCl_2$, and the oligonucleotide staple strands designed in caDNAno and ordered from a commercial vendor (Eurofins Genomics), so that each staple was at excess (200 nM) compared to the scaffold. A 6.5 day thermal ramp of rapid heating to 65 degrees C and slow cooling was applied to facilitate self assembly. Several versions of the LPP were folded where biotinylated oligonucleotide staples included in the folding reactions varied based on desired linker length and desired number of ligands on the platform. Figures 12 and 13 display the varied linker lengths, quantities, and spatial arrangements.

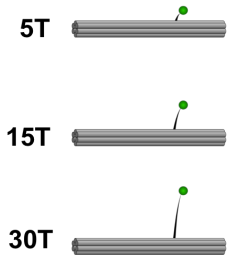

Figure 12: Linker length can be controlled as desired, for example linker length of 5 base-pairs (5T), 15 base-pairs (15T), and 30 base-pairs (30T.)

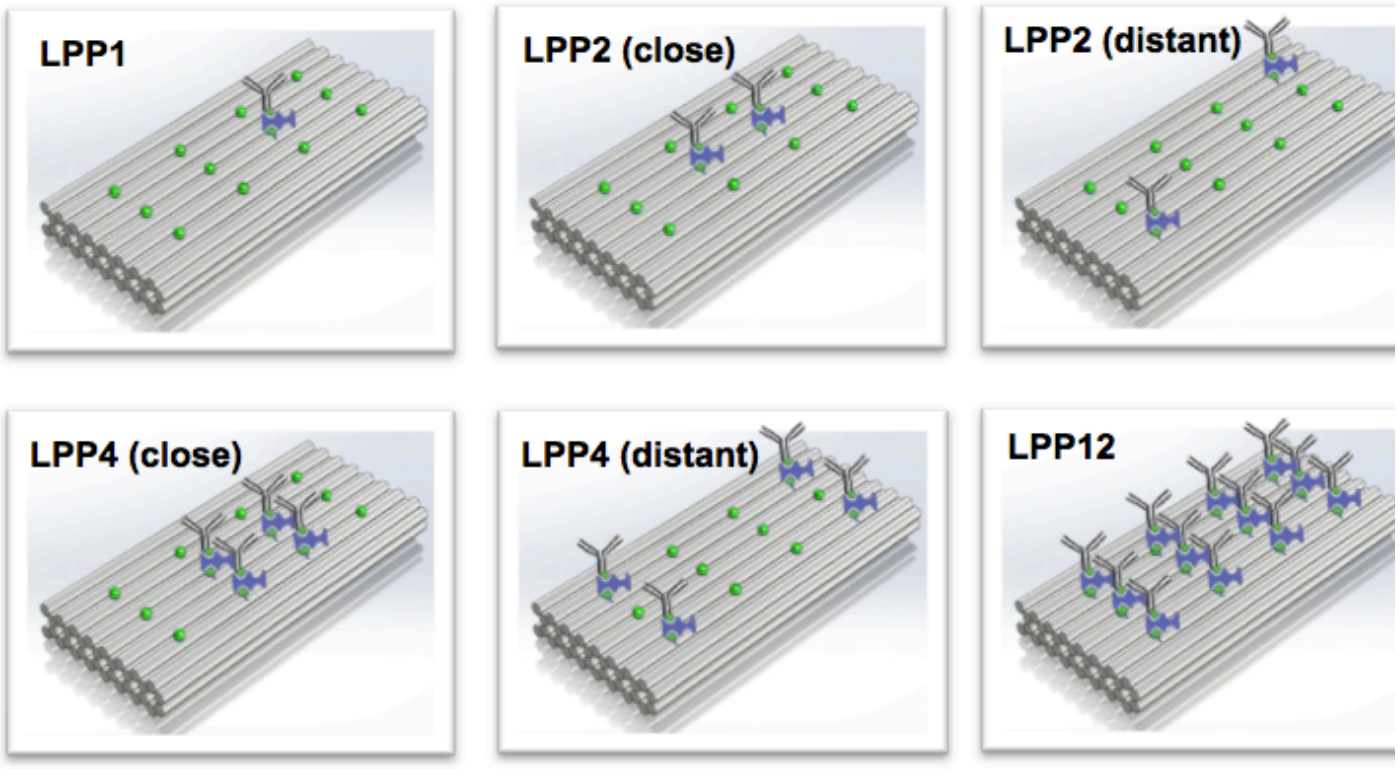

Figure 13: Number of attached ligands and locations of attachment can be controlled as desired. For example LPP1, LPP2 (close), LPP2 (distant), LPP4 (close), LPP4 (distant), LPP12, or any other combination of the 12 ligand locations.

After the self-assembly reaction, reactant products were subjected to purification to remove excess staple strands. The folding reaction was added in equal volume to 15% polyethylene glycol (PEG) 8000 and this mixture was centrifuged at 16000 g for 30 minutes at 4 degrees C. The supernatant containing the excess ssDNA oligos was removed and discarded while the pellet containing the folded DNA origami structures was resuspended in 1X FOB and 18mM $MgCl_2$. To confirm well-folded nanostructures, folding reaction products were also subjected to gel electrophoresis, purification, and transmission electron microscopy described below.

2.3 Functionalization with Streptavidin and Antibody

UV absorption was used to measure the concentration of the DNA origami nanostructures. Streptavidin was added in 40-fold molar excess and incubated for 1 hour at room temperature. Biotinylated antibodies were added at 10-fold molar excess and incubated overnight at 4 degrees C.

2.4 Verification via Gel Electrophoresis

To verify properly folded structures, gel electrophoresis was used. The products of the folding reaction were run through a 2% agarose gel in the presence of 0.5X TBE and 11mM $MgCl_2$. Gels were run at 70V for 1-4 hours to allow time for band separation. The resulting gel was imaged and leading bands were excised.

2.5 Verification via Transmission Electron Microscopy

To further verify, unfunctionalized structures, structures with streptavidin, and structures with streptavidin and antibody were imaged via transmission electron microscopy (TEM.) The products of the gel electrophoresis were placed on copper mesh grids and negatively stained with uranyl formate as previously described in Castro, Nat. Method, 2011[40]. The nanostructures were imaged at an electron acceleration voltage of 80kV on a Tecnai G2 BioTWIN TEM.

2.6 Fluorescent Microscopy: B cells over 20 hours

To evaluate functionalized nanostructure-anti-CD40 induced NF-κB response, single cell epifluorescence imaging was employed on CH12.LX B cells[41]. Nucleofection (Amaxa program 0-

003) with 2.5-5 μg of Cignal GFP-NF-κB reporter construct (SA Biosciences) was used to transfect 1 million CH12.LX B cells. After transfection, cells were incubated overnight at 37 degrees C and 5% CO_2 in complete medium (RPMI 1640 (CellGrow) media containing 10% FBS (Atlas Biologicals), 20mM HEPES (Gibco), 100 U/ml penicillin (Gibco), 100 μg/ml streptomycin (Gibco) and 2mM L-glutamine (Gibco), and 50μM 2-ME (Sigma Aldrich)) and then resuspended in clear RPMI 1640 (Gibco), 0.5% FBS, and 2% penicillin/streptomycin/L-Glutamine. Cells were plated in live cell imaging wells (Thermo Scientific) and functionalized LPPs were added at 600 pM. The sample was incubated in the presence of 7-AAD (1:100) in a stage-top incubator at 37 degrees C and 5% CO_2 throughout the 20 hours of imaging on a Nikon Eclipse Ti2. The level of NF-κB cellular response was quantified via epiflorescence imaging emission of the GFP reporter at 488 nm excitation. Cell viability was determined via epifluorescence imaging emission of the 7-AAD at 561 nm excitation.

2.7 Fluorescent Microscopy: T cells over 5 minutes

To begin evaluating functionalized nanostructure-anti-CD3 induced calcium response, single cell epifluorescence imaging was employed. Jurkat T cells (2 million/mL) cultured in altered complete RPMI (RPMI 1640 (CellGrow) media containing 10% FBS (Atlas Biologicals), 100 U/ml penicillin (Gibco), 100 μg/ml streptomycin (Gibco) and 2mM L-glutamine (Gibco)) were dyed at 1 mM Fluo-4 AM (Life Technologies) and incubated in HBSS for 30 minutes at 37 degrees C and 5% CO_2. Cells were plated in live cell imaging wells (Thermo Scientific) and incubated for an additional 45 minutes at the conditions described above. During imaging, the sample was incubated in a stage-top incubator at 37 degrees C and 5% CO_2 on a Nikon Eclipse

Ti2. After one minute of imaging, the stimulus was added. Stumuli included soluble anti-CD3 (OKT3)-biotin (eBioscience) at 10 μg/mL and a buffer only negative control. The level of intracellular calcium response was quantified via epiflorescence imaging with 488 nm excitation.

Chapter 3: Results

3.1 Gel Electrophoresis

Figure 14 depicts typical results from gel electrophoresis purification of LPP nanostructures. Several samples were run on the gel including a 1kb reference ladder (New England Biolabs) on the far left and far right wells, the 7560 base scaffold in the second lane, resulting in one tight band, and the folded structure bands in lanes 3-14. Because smaller DNA objects pass through the agarose gel more quickly, the gel results in separation of structures by size. The lanes with the folded structures included a large bright smear corresponding to the excess staples that ran the farthest, a narrow bright band corresponding to the well folded structure, and a faint smear between the well and structure band corresponding to misfolded or aggregated structures. Well-folded structures form a tight band that runs slightly faster than the reference scaffold because they are more compact than the unfolded scaffold.

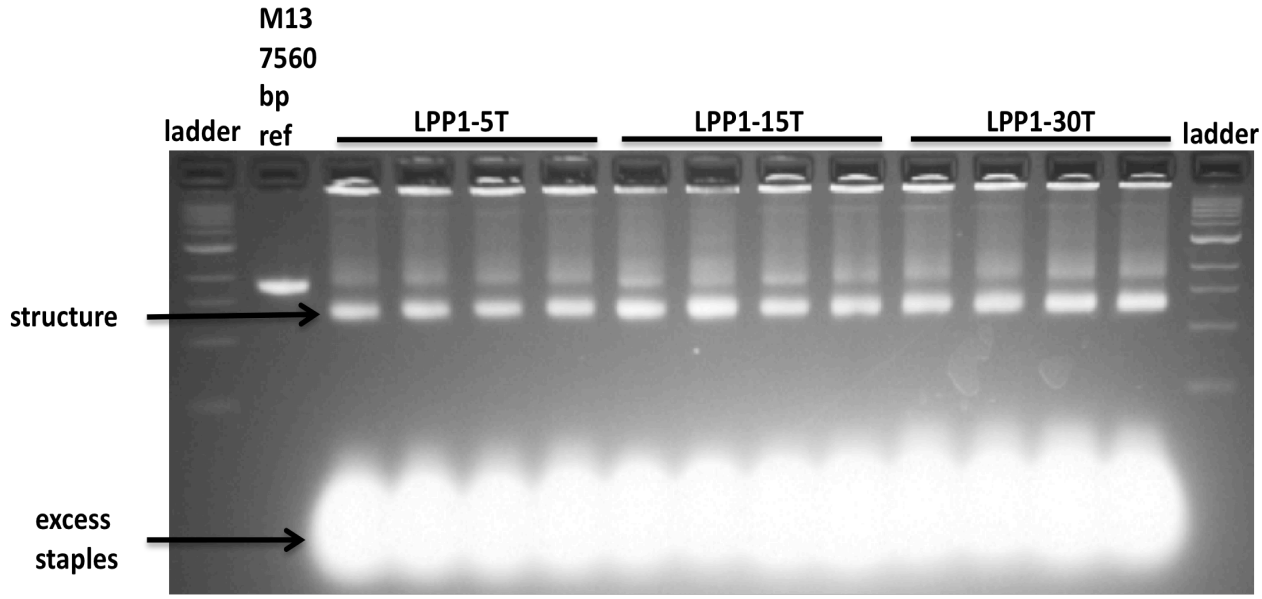

Figure 14: Gel Electrophoresis. LPP1-5T, LPP1-15T, and LPP1-30T underwent gel electrophoresis with ladder controls and a 7560 base-pair reference control.

3.2 Transmission Electron Microscopy

To further verify well-folded structures, structures were imaged via transmission electron microscopy (TEM.) As shown in Figure 15 and Figure 16, transmission electron microscopy resulted in visualization of LPPs with proper streptavidin and antibody attachment number and location, as shown in proper quantity and location on LPP1, LPP2, and LPP4. In addition, TEM can verify antibody attachment to streptavidin, as shown in Figure 16. This figure depicts LPP1 with streptavidin and with streptavidin/antibody attachment.

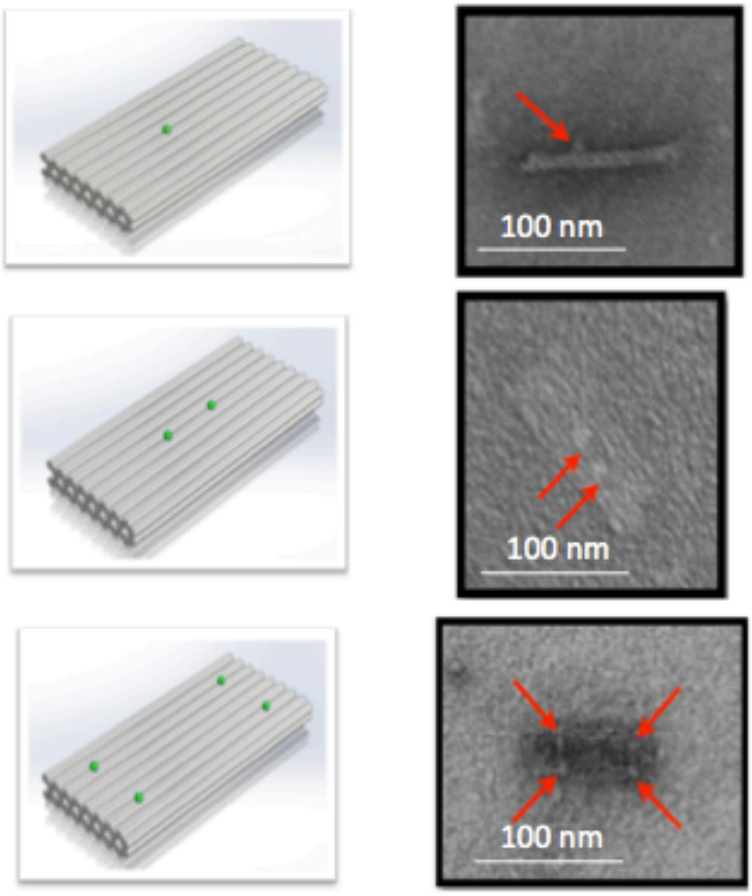

Figure 15: TEM Streptavidin Attachment. Cartoon image (left) and TEM image (right) showed that streptavidin (marked with red arrows) attaches in the number and location that is expected.

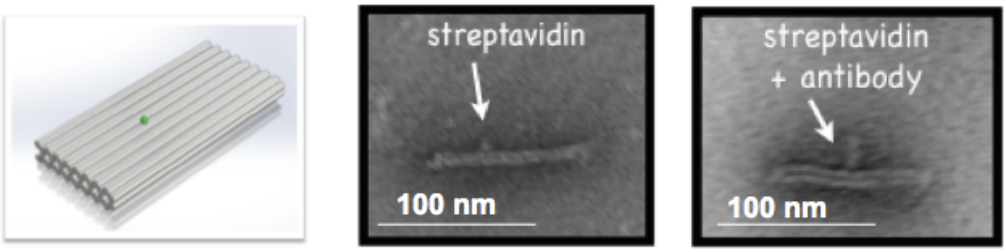

Figure 16: TEM streptavidin and antibody attachment. Cartoon image (left), TEM image of streptavidin only added (middle), and TEM image of streptavidin and antibody (right) showed that antibody attaches as expected.

3.3 Fluorescent Microscopy: B cells over 20 hours

To analyze the functionalization of the structures, fluorescent microscopy was completed. This examination resulted in observation of an increased response in reporter fluorescence, indicating increased production of GFP due to NF-κB activation in response to CD40L functionalized nanostructures. Experiments were controlled with a none negative control, a platform with streptavidin only, and a platform with an isotype control antibody attached.

As shown in Figures 17-21, a ~4-fold change existed compared to controls after 20 hours. In Figure 17, a qualitative change is clearly observable between LPP2 with anti-CD40 relative to controls at 20 hours. In Figure 18, a ~4-fold quantitative change induced by LPP2 anti-CD40 is shown after 20 hours relative to the controls. Figure 19 displays a ~3-fold change induced by LPP11 anti-CD40 compared to the controls. Finally, in Figure 20, a ~2 fold change induced by LPP12 anti-CD40 is shown at 20 hours relative to the controls. Therefore, a downward trend existed in that LPPs with more ligands produce less response than platforms with fewer ligands.

In addition, as shown in Figure 22, the response was concentration dependent. While the concentration of the structures was unknown, when the structures were added at a higher concentration (1:10 indicates the volume of structures added to volume of cell solution) and subsequent ten-fold serial dilutions (1:100 and 1:1000) were completed, a higher magnitude response was observed when LPP structures were added at a higher concentration. Figure 23

shows a decreasing response with increasing concentration of inhibitor, Bay-11-7082, confirming that the response is capable of being inhibited by an NF-κB cascade blocker.

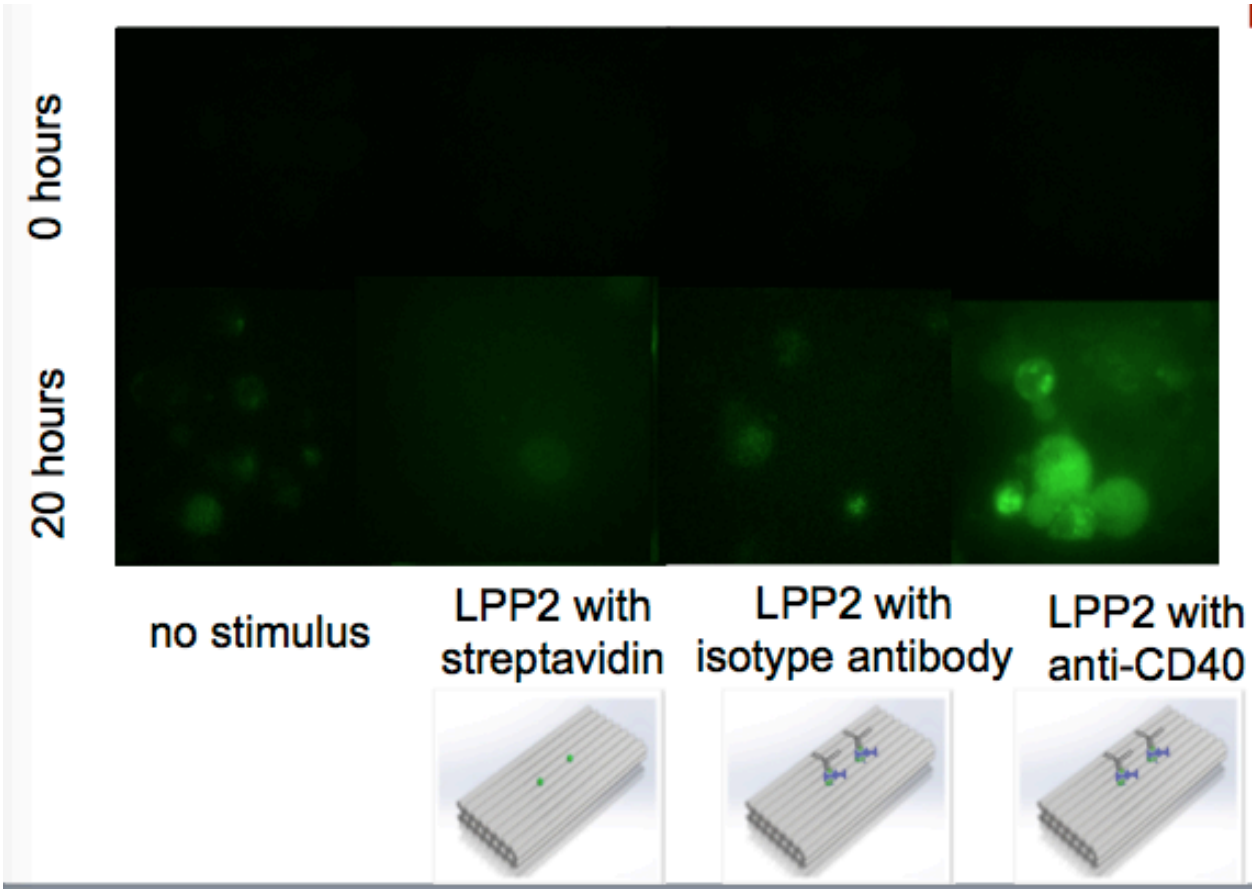

Figure 17: Qualitative functional response. A qualitative difference is exhibited between functionalized structures (on right) and controls (all others) after 20 hours. The relative level of fluorescence corresponds to GFP production via CD40L activation.

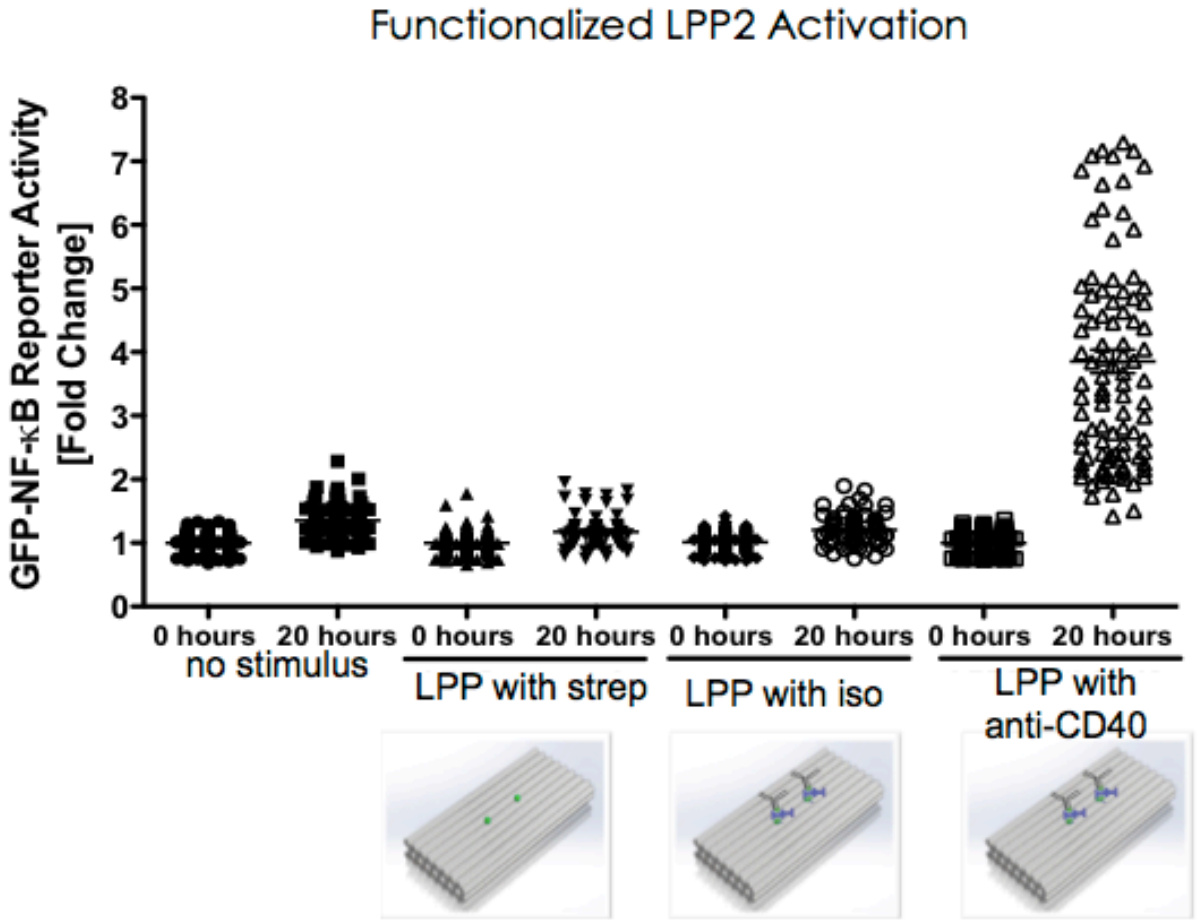

Figure 18: Fluorescent microscopy to measure functional response in B cells. Functionalized LPP2-5T (right) with controls (no stimulus, LPP with streptavidin, and LPP with isotype control antibody.) The level of GFP-NF-κB was measured on individual cells per condition and the data is presented as the intensity mean Fold Change ± SEM relative to 0 hours for each condition. Images and data represent two experiments.

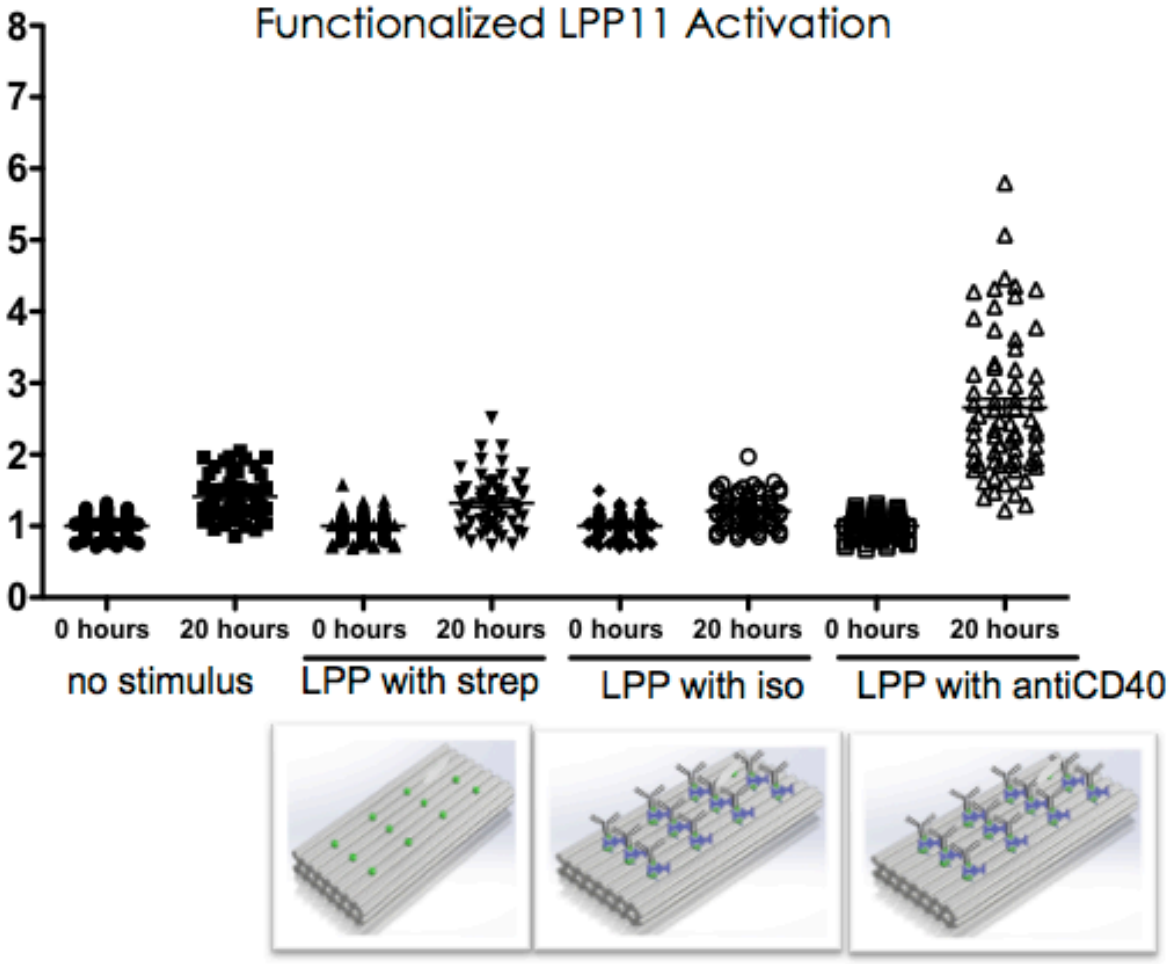

Figure 19: Fluorescent microscopy to measure functional response in B cells. Functionalized LPP11-5T (right) with controls (no stimulus, LPP with streptavidin, and LPP with isotype control antibody.) The level of GFP-NF-κB was measured on individual cells per condition and the data is presented as the intensity mean Fold Change ± SEM relative to 0 hours for each condition. Images and data represent two experiments.

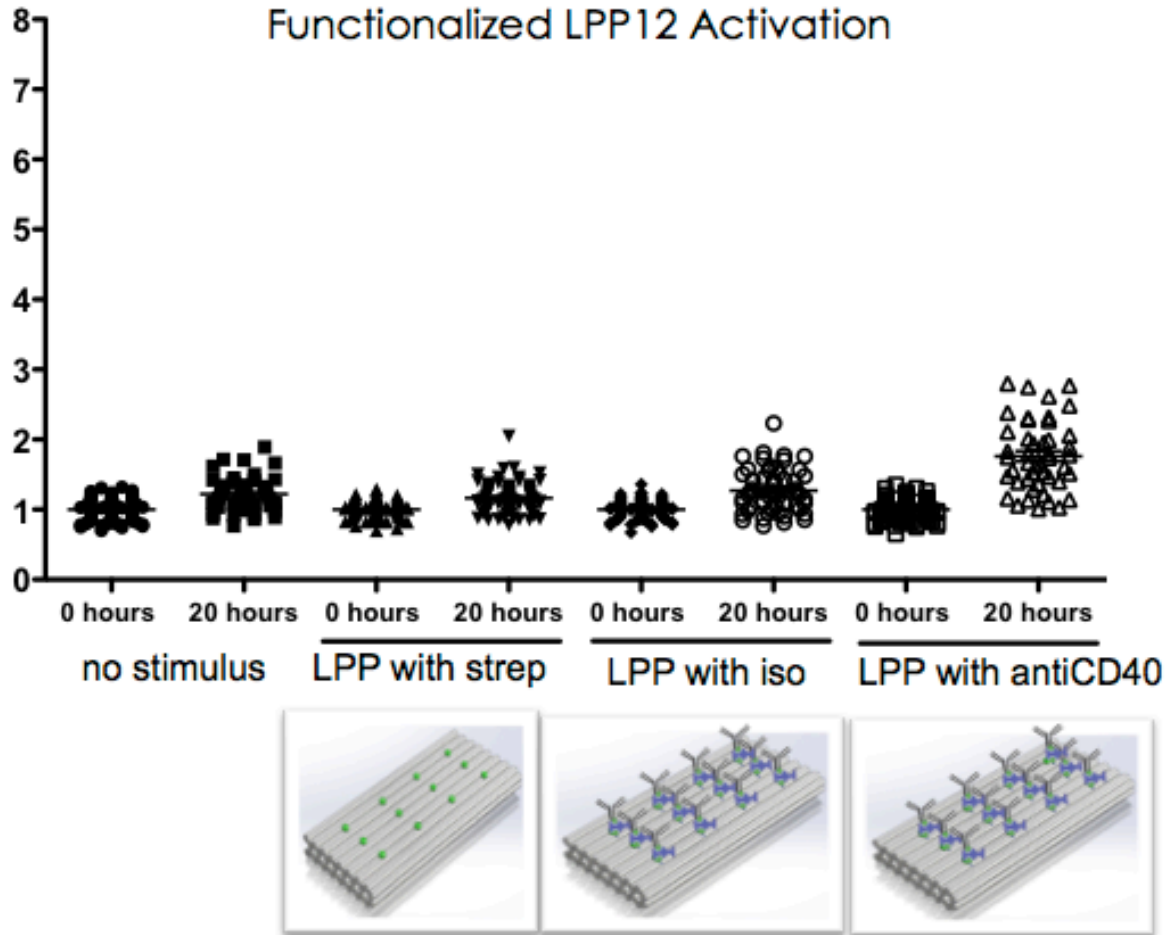

Figure 20: Fluorescent microscopy to measure functional response in B cells. Functionalized LPP12-5T (right) with controls (no stimulus, LPP with streptavidin, and LPP with isotype control antibody.) The level of GFP-NF-κB was measured on individual cells per condition and the data is presented as the intensity mean Fold Change ± SEM relative to 0 hours for each condition. Images and data represent two experiments.

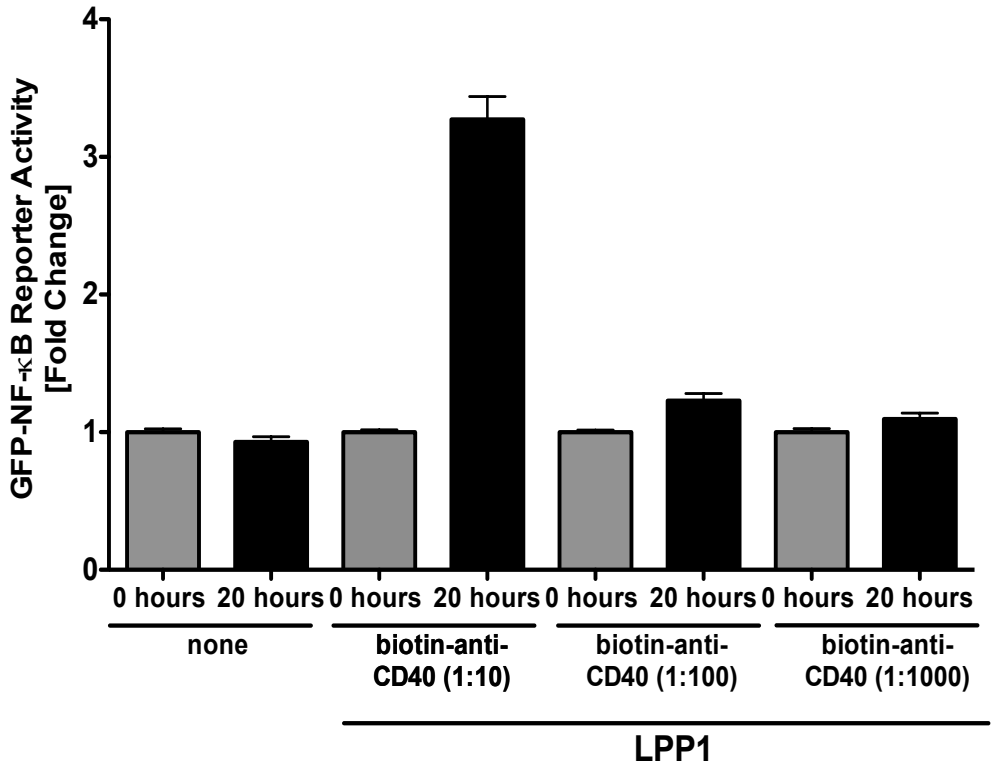

Figure 21: Fluorescent microcopy to measure concentration dependence in B cells. Anti-CD40 functionalized LPP1-5T showed a concentration dependent change in signal induction. The level of GFP-NF-κB was measured on at least 40 cells per condition and the data is presented as the intensity mean Fold Change ± SEM relative to 0 hours for each condition. Images and data represent one experiment.

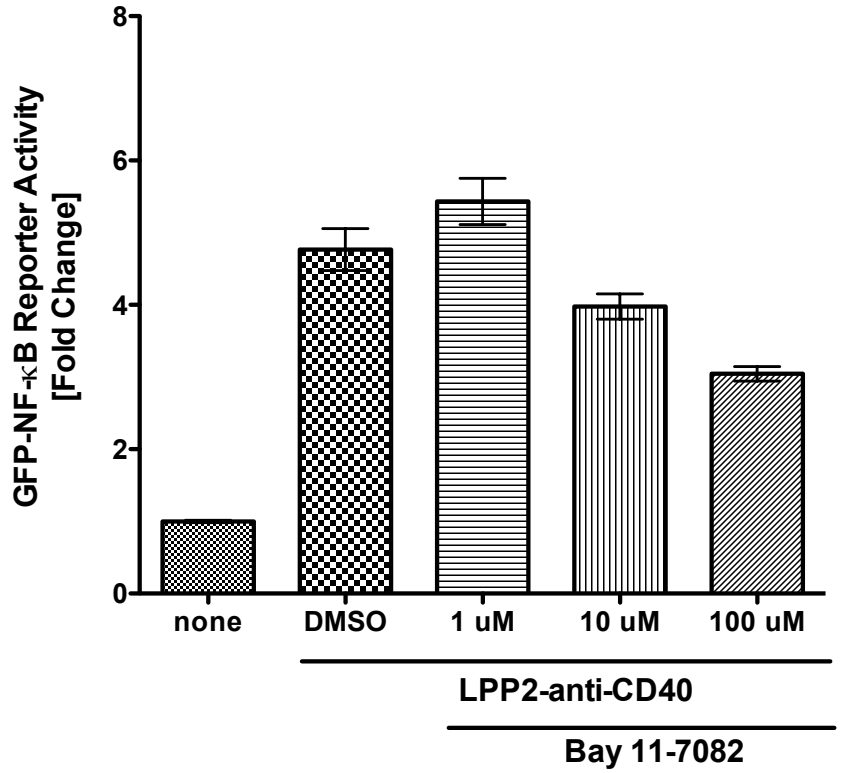

Figure 22: Fluorescent microscopy to measure inhibition of signal in B cells. anti-CD40 functionalized LPP2-5T showed an ability to be inhibited by Bay-11-7082.

3.5 Fluorescent Microscopy: T cells over 5 minutes

To further support that this nanostructure is an effective way to study cell communication, the process is shown on an additional cell type, receptor-ligand interaction, and subsequent cellular response. Fluorescent microscopy showed an increased response in 488 fluorescence, indicating influx of intracellular calcium after the addition of soluble anti-CD3. This experiment was controlled with a none negative control.

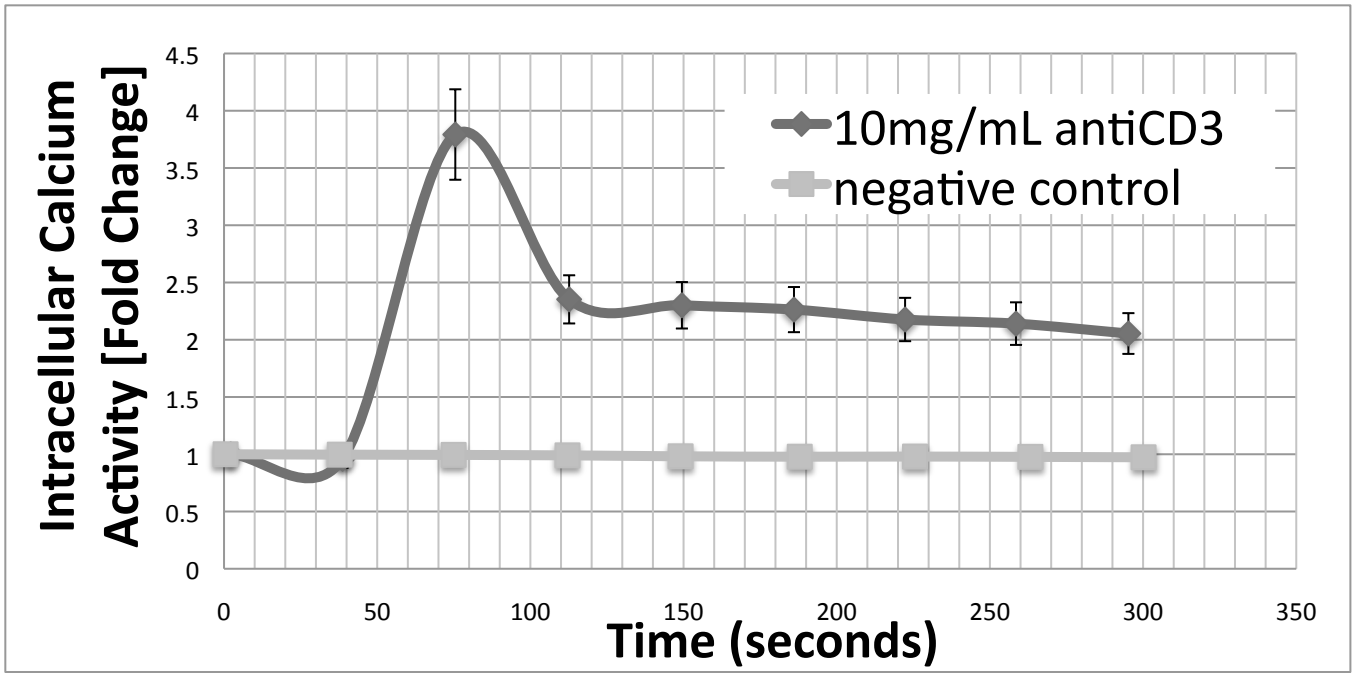

Figure 23: Fluorescent microscopy to measure functional response in T cells. Soluble anti-CD3-biotin was added to T cells at 60 seconds. The level of intracellular calcium was measured on at least 150 cells per condition and the data is presented as the intensity mean Fold Change ± SEM relative to 0 hours for each condition. Data represents one experiment.

Chapter 4: Conclusions and Future Work

Cell to cell communication is relevant in the development of well-targeted, effective cancer therapeutics against specific pro-growth and survival intracellular signaling pathways. Current methods to study cell-cell communication fail to ensure correct ligand immobilization and lack the ability to study the influence of ligand spatial arrangement and range of motion. In order to establish a ligand-receptor examination method that more closely mimics natural cell-cell communication, well-defined signaling pathways should be examined. Two well-defined pathways, CD40 induction of NF-κB in B cells and calcium influx via CD3 engagement in T cells, are such examples and are in the process of being examined using a novel nanoengineering technique.

This technique synthesizes a nanoplatform using a method called scaffolded DNA. This platform correctly immobilizes a ligand and makes it possible to study the influence of ligand spatial arrangement and local flexibility of the ligand. The LPP nanostructure has shown that it can be folded and functionalized with streptavidin and antibody in the quantity, spatial arrangement, and range of motion that is desired. In B cells, it has shown to be functional and induce a functional response at a ~4-fold magnitude to relevant controls. While the T cell TCR data is preliminary and LPP nanostructures have not yet been tested in this system, the soluble ligand response is comparable in time scale and magnitude to established published responses in similar systems[42,43].

Future experiments will be designed to assess the importance of ligand quantity and range of motion. On both T cell and B cell systems, relevance of ligand quantity and

concentration will be examined by varying both concentration of LPP structures and ligand quantity on the LPP structure from one ligand (LPP1) to twelve ligands (LPP12.) Examination of ligand range of motion should also be tested in the T cell and B cell system by comparing LPP1-5T (ligand attached by 5 base linker) to LPP1-15T (ligand attached by 15 base linker) and LPP1-30T (ligand attached by 30 base linker).

To ensure that the functional response is caused by the signaling cascades expected, inhibitor tests should be completed in both systems. In addition to the immortalized cell lines used, primary B cells and T cells should be tested in order to ensure physiological relevance. Finally, to further confirm the results found on a single cell level using fluorescence imaging, flow cytometry and flourometer analysis should be employed to visualize the response on a population level.

Ultimately, if proteins or other molecules can be attached to this nanostructure to cause a cellular functional response, then these nanostructures can be used both to examine and understand signaling cascades as well as to deliver therapeutic messages. For example, these structures can be used to examine a poorly understood ligand-receptor interaction that may be relevant in cancer pathology. Furthermore, if the platform can deliver a protein that leads to cell death, then these structures can be used therapeutically to initiate cancer cell death.

Bibliography

[1] Cancer Prevention and Control by Centers for Disease Control and Prevention. Retrieved June 4, 2014 from http://www.cdc.gov/cancer/dcpc/resources/features/worldcancerday/

[2] Institute, N.C. (2013, June 14). *Surveillance Epidemiology and End Results.* Retrieved September 18, 2013, from http://seer.cancer.gov/csr/1975_2010/sections.html

[3] Sawyers, Charles. "Targeted Cancer Therapy." *Nature* 432.7015 (2004): 294-97.

[4] Scitable: by Nature Education. *Cell Signaling.* Retrieved September 18, 2013 from www.nature.com/scitable/topicpage/cell-signaling-14047077

[5] Pray, L. "Discovery of DNA Structure and Function: Watson and Crick." *Nature Education* 1.1:100 (2008).

[6] Pray, L. "Discovery of DNA Structure and Function: Watson and Crick." *Nature Education* 1.1:100 (2008).

[7] Seeman, N. "Nucleic Acid Junctions and Lattices." *Journal of Theoretical Biology* 99 (1982):237-247.

[8] Chen, J., Seeman, N. "Synthesis from DNA of a molecule with the connectivity of a cube." *Nature*. 350 (1991):631-633.

[9] Linko, V., Dietz, H. "The enabled state of DNA nanotechnology." *Current Opinion in Biotechnology.* 24 (2013):555-561.

[10] Rothemund, Paul. "Folding DNA to create nanoscale shapes and patterns." *Nature* 440 (2006):297-302.

[11] Rothemund, Paul. "Folding DNA to create nanoscale shapes and patterns." *Nature* 440 (2006):297-302.

[12] Castro, C., Kilchherr, F., Kim, D, Shiao, E., Wauer, T., Wortmann, P., Bathe, M., Dietz, H. "A primer to scaffolded DNA origami." *Nature Methods.* 8(2011):221-229.

[13] Kim, S.T., Takeuchi, K., Sun, Z.Y.J., Touma, M., Castro, C.E., Fahmy, A., Lang, M.J., Wagner, G., Reinherz, E.L. "The αβ T Cell Receptor Is an Anisotropic Mechanosensor." *Journal of Biological Chemistry* 284.45 (2009): 31028-37.

[14] Dykstra, M., Cherukuri, A., Sohn, H.W., Tzeng, S.J., Pierce, S. "Location is Everything: Lipid Rafts and Immune Cell Signaling." *Annual Review on Immunology* 21 (2003):457-81.

[15] Homberg, A., Blomstergren, A., Nord, O., Lukacs, M., Lundeberg, J., Uhlen, M. "The biotin-streptavidin interaction can be reversibly broken using water at elevated temperatures." *Electrophoresis* 26.3 (2005): 501-10.

[16] Alberts. *Molecular and Cell Biology.* Edition 5 (2007.) Chapter 25: 1539-1541.

[17] Alberts. *Molecular and Cell Biology.* Edition 5 (2007.) Chapter 25: 1539-1541.

[18] Bishop, G., Hostager, B. "The CD40-CD154 interaction in B cell-T cell liaisons." *Cytokine and Growth Factor Reviews.* 14, 3-4 (2003):297-309.

[19] Bergwelt-Baildon, M., Maecker, B., Schultze, J., Gribben, J. *"CD40 activation: potential for specific immunotherapy in B-CLL.* 15(2004):853-857.

[20] Graham, J., Arcipowski, K., Bishop, G. "Differential B-lymphocyte regulation by CD40 and its viral mimic, latent membrane protein 1." *Immunological Reviews* 237.1 (2010): 226-248.

[21] Graham, J., Arcipowski, K., Bishop, G. "Differential B-lymphocyte regulation by CD40 and its viral mimic, latent membrane protein 1." *Immunological Reviews* 237.1 (2010): 226-248.
[22] Memet, S. "NFkB functions in the nervous system: from development to disease." *Biochemical Pharmacology* 72 (2006): 1180-1195.
[23] Dolcet, X., Llobet, D., Pallares, J., Matias-Guiu, X. "NF-kB in development and progression of human cancer." *Virchows Archiv* 446.5 (2005): 475-82.
[24] Hooper, C. "Overview of NFkB signaling." Abcam. Retrieved June 4, 2014 from http://www.abcam.com/?pageconfig=resource&rid=11255&pid=10629
[25] Smith-Garvin, J.E., Koretzky, G.A., Jordan, M.S. "T Cell Activation." *Annual Review on Immunology* 27 (2009): 591-619.
[26] Dykstra, M., Cherukuri, A., Sohn, H.W., Tzeng, S.J., Pierce, S. "Location is Everything: Lipid Rafts and Immune Cell Signaling." *Annual Review on Immunology* 21 (2003):457-81.
[27] Natkanski, E., Lee, W., Mistry, B., Casal, A., Molloy, J., Tolar, P. "B Cells Use Mechanical Energy to Discriminate Antigen Affinities." *Science* 340.5140 (2013):1587-90.
[28] Kim, S.T., Takeuchi, K., Sun, Z.Y.J., Touma, M., Castro, C.E., Fahmy, A., Lang, M.J., Wagner, G., Reinherz, E.L. "The αβ T Cell Receptor Is an Anisotropic Mechanosensor." *Journal of Biological Chemistry* 284.45 (2009): 31028-37.
[29] Smith-Garvin, J.E., Koretzky, G.A., Jordan, M.S. "T Cell Activation." *Annual Review on Immunology* 27 (2009): 591-619.
[30] Oh-hora, M., Rao, A. "Calcium signaling in lymphocytes." *Annual Review of Immmunology.* 20 (2008):250-8
[31] Smith-Garvin, J.E., Koretzky, G.A., Jordan, M.S. "T Cell Activation." *Annual Review on Immunology* 27 (2009): 591-619.
[32] Alberts. *Molecular and Cell Biology.* Edition 5 (2007.) Chapter 25: 1540-1551.
[33] Smith-Garvin, J.E., Koretzky, G.A., Jordan, M.S. "T Cell Activation." *Annual Review on Immunology* 27 (2009): 591-619.
[34] Kim, S.T., Takeuchi, K., Sun, Z.Y.J., Touma, M., Castro, C.E., Fahmy, A., Lang, M.J., Wagner, G., Reinherz, E.L. "The αβ T Cell Receptor Is an Anisotropic Mechanosensor." *Journal of Biological Chemistry* 284.45 (2009): 31028-37.
[35] Bergwelt-Baildon, M., Maecker, B., Schultze, J., Gribben, J. *"CD40 activation: potential for specific immunotherapy in B-CLL.* 15(2004):853-857.
[36] Warner, K., Weit, N., Crispatzu, G., Admirand, J., Jones, D. "T-Cell Receptor Signaling in Peripheral T-Cell Lymphoma – A Review of Patterns of Alterations in a Central Growth Regulatory Pathway." *Current Hematologic Malignancy Report.* 163, 10 (2013):163-172.
[37] Siegel, R., Naishadham, D., Jemal, A. "Cancer Statistics, 2012." *Cancer Journal for Clinicians* 62 (2012): 10-29.
[38] Douglas, S., Marblestone, A., Teerapittayanon, S., Vazquez, A., Church, G., Shih, W. "Rapid prototyping of 3D DNA-origami shapes with caDNAno." *Nucleic Acids Research.* 10.1093 (2009):1-6.
[39] Castro, C., Kilchherr, F., Kim, D, Shiao, E., Wauer, T., Wortmann, P., Bathe, M., Dietz, H. "A primer to scaffolded DNA origami." *Nature Methods.* 8(2011):221-229.
[40] Castro, C., Kilchherr, F., Kim, D, Shiao, E., Wauer, T., Wortmann, P., Bathe, M., Dietz, H. "A primer to scaffolded DNA origami." *Nature Methods.* 8(2011):221-229.

[41] Bishop, G.A., Haughton, G. “Induced differentiation of a transformed clone of Ly-1+ B cells by clonal T cells and antigen.” *Proc. Natl. Acad. Sci.* 83(1986):7410-7414.
[42] Xavier, R., Brennan, T., Li, Q., McCormack, C., Seed, B. “Membrane Compartmentation Is Required for Efficient T Cell Activation.” *Immunity*. 8, 6 (1998):723-732.
[43] Bailey, S., Macardle, P. “A flow cytometric comparison of Indo-1 to fluo-3 and Fura Red excited with low power lasers for detecting Ca^{2+} flux.” *Journal of Immunological Methods.* 311(2006)220-225.